Journal of the Korean Society of Surveying, Geodesy, Photogrammetry and Cartography
Vol. 41, No. 5, 395-405, 2023
https://doi.org/10.7848/ksgpc.2023.41.5.395

ISSN 1598-4850(Print)
ISSN 2288-260X(Online)
Original article

Improving The Accuracy Of Digital Elevation Model Using Hopfield Neural Network With Additional Elevation Point Dataset

Nguyen, Quang Minh[1] · La, Phu Hien[2] · Nguyen, Thi Thu Huong[3] · Hoang, Ngoc Ha[14]

Abstract

In this paper, a new approach for the improvement of accuracy in DEMs (Digital Elevation Models) was proposed. While algorithms such as bilinear, bicubic, Kriging, and the HNN (Hopfield neural network) model can enhance the accuracy of DEMs, especially those derived from global data sources such as SRTM, ASTER, etc., the inclusion of additional elevation data can further improve the accuracy of the DEM. In this paper, a newly proposed resolution enhancing HNN model with the incorporation of elevation adjustment functions and variations in constraint conditions was developed and evaluated. The evaluation of the model was implemented in Cao Bang using SRTM 30m DEM data in a 1650m × 1344m area, with 130 elevation points used for accuracy enhancement and 64 points used for evaluation. The test results show an increase in accuracy of up to 40% in terms of both roots mean square error and mean absolute error when the additional elevation points were used. It has also been discovered that a zoom factor of 4 provides the best optimization in terms of balancing accuracy and computing cost for the newly proposed HNN downscaling algorithm. The results indicate that the model has the potential to be applied in practice to enhance the accuracy of DEMs, especially global DEMs after additional evaluation.

Keywords : DEM, downscaling, Hopfield Neural Network, resampling

1. Introduction

The accuracy of a DEM (Digital Elevation Model) is one of the crucial factors in terrain analysis. However, some commonly used global DEMs such as SRTM (Shuttle Radar Topography Mission) and ASTER (Advanced Spaceborne Thermal Emission and Reflection Radiometer) with a spatial resolution of 30m often suffer from limitations in accuracy when representing terrain, especially in the areas with complex topography and significant elevation differences (Courty *et al*., 2019; Uuemaa *et al*., 2020). Therefore, various methods have been used to improve the accuracy of digital elevation models, including conventional methods such as bilinear resampling, bicubic interpolation (Wu *et al*., 2008), Kriging (Grohmann & Steiner, 2008), or the more unconventional approach such as Hopfield neural network downscaling (HNN)

Received 2023.09.28, Revised 2023.10.06, Accepted 2023.10.25
1) Corresponding Author, Faculty of Geomatics and Land Administration, Assoc. Prof.,, Hanoi University of Mining and Geology, Hanoi, Vietnam (E-mail: nguyenquangminh@humg.edu.vn/ng.q.minh@gmail.com)
2) Member, Faculty of Water Resource, Thuyloi University, Hanoi, Vietnam (E-mail: laphuhien@tlu.edu.vn)
3) Member, Faculty of Geomatics and Land Administration, Senior Lecturer, Hanoi University of Mining and Geology (E-mail: nguyenthithuhuong@humg.edu.vn)
4) Member, Faculty of Geomatics and Land Administration, Prof., Hanoi University of Mining and Geology, Hanoi, Vietnam (E-mail: hoangngocha@humg.edu.vn)

(Q. M. Nguyen *et al*., 2019). The accuracy of DEM data can also be enhanced by using multiple DEMs with lower accuracy to create a higher-accuracy DEM, such as combining SRTM and ASTER DEMs (Pham *et al*., 2018).

One of the widely applied methods to improve the accuracy of global DEM data is the use of supplementary data, especially elevation data, to refine the existing DEM data. The supplementary data used can be land cover data to correct elevation errors caused by vegetation, as in the study by Yamazaki *et al*. (Yamazaki *et al*., 2017), or studies that utilize river and canal network information as drainage convergence points (the lowest points in a specific area) to adjust the DEM, as in the research conducted by Bhuyian *et al*. (Bhuyian *et al*., 2015). Similarly, in the study by Jana *et al*. (Jana *et al*., 2007), a network of water outflow systems is employed to enhance the accuracy of the DEM, enabling a more accurate representation of the terrain surface.

One of the supplementary data sources used to improve the accuracy of DEM are additional elevation points, where algorithms utilizing geostatistical conflation techniques are employed to incorporate the data to improve the accuracy of DEMs. Paredes-Hernández *et al*. (Paredes-Hernández *et al*., 2010) used a geostatistical approach to adjust various global DEMs such as ASTER GDEM, Inegi DEM, and SRTM DEM, demonstrating that the algorithm reduced the root mean square error of the DEM ranging from 0.5m to 2m depending on the input DEM type. Similarly, Tang *et al*. (Tang *et al*., 2014) utilized a multi-point geostatistical method with 250 elevation points to enhance the accuracy of the SRTM DEM in Zhangye City, China. The results showed that when employing the additional elevation points with this algorithm, the mean square error of the 30m SRTM DEM decreased by an amount range from 0.5m to 3m, depending on the Kriging method.

In enhancing the accuracy of DEMs through resampling techniques, the method of using the Hopfield neural network has several advantages and yields results with higher accuracy compared to other methods such as bilinear, bicubic, or Kriging interpolation (Q. M. Nguyen *et al*., 2019). One of the advantages of this method is its ability to integrate the original DEMs with the other data sources by incorporating additional goal functions or constraints (M. Q. Nguyen *et al*., 2006) to generate DEMs with higher resolution than the original resolution. In this study, a new algorithm was proposed to enable the integration of high-accuracy elevation points into the resolution-enhancement model using the Hopfield neural network. The goal is to improve the accuracy of the DEM more than the traditional methods of resampling and HNN (Hopfield neural network) downscaling. This proposed model is tested with the data collected in an area located in Cao Bang Province, Vietnam.

2. Methods

2.1 DEM downscaling using HNN

The proposed method developed based on the HNN model aims to increase the resolution of a DEM using the previously used HNN model for DEM downscaling proposed by Nguyen et. al. (Q. M. Nguyen *et al*., 2019). The main idea of the method is to divide the pixels in the original DEM into smaller sub-pixels, corresponding to neurons in the HNN model. The scaling factor (f) is used to determine the ratio between the size of the higher resolution DEM′s sub-pixels and the original pixels. In the presented example in Figure 1, the size of the DEM region is 2×2 pixels. Each pixel is divided into 4×4 smaller sub-pixels, resulting in a new DEM with a size of 8×8 sub-pixels, corresponding to 8×8 neurons in the HNN. Specifically, this method utilizes a linear activation function of the HNN to optimize the elevation values of the higher resolution pixels based on the elevation data from the original DEM. This optimization process helps to recreate details and improve the resolution of the new DEM.

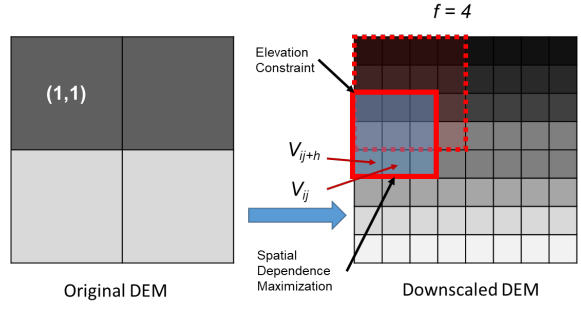

Fig. 1 Downscaling model using Hopfield neural network.

Fig. 1 is presented to illustrate the process of increasing the

resolution of a DEM. This process can be applied throughout the entire DEM to enhance the overall resolution of the digital elevation model.

The HNN DEM downscaling model operates based on goal functions and elevation constraint. The goal function of this neural network is based on the principle of maximizing spatial dependency, where neighboring pixels in the DEM model tend to have similar elevations. This is determined by assessing the similarity of elevation values among the sub-pixels in the DEM model using a semi-variogram function, as follows:

$$\gamma(h) = \frac{1}{2N(h)} \sum_{1}^{N(h)} \left[v_{ij} - v_{ij+h}\right]^2 \quad (1),$$

Where $\gamma(h)$ represents the variogram value for each distance between two points (two sub-pixels), h is the distance between pairs of points. v_{ij} and v_{ij+h} are the corresponding elevation values at points i, j and $(i, j) + h$, $N(h)$ is the number of point pairs.

If the elevation values of these points are similar, the value of the variogram function will be small. Therefore, to maximize spatial dependency, it is necessary to modify the elevation values v_{ij} and $v_{(ij+h)}$ in such a way that the variogram value $\gamma(h)$ is minimized.

To determine the values of v_{ij} and $v_{(ij+h)}$ according to the above-mentioned principle, you need to find the minimum value of the variogram by setting the derivative of the variogram function equal to zero:

$$\partial\gamma(\mathrm{h})/\partial\mathrm{v} = 0 \quad (2)$$

Setting the derivative of the variogram function equal to zero, it is possible to find the optimal values of v_{ij} and $v_{(ij+h)}$ that minimize the variogram and maximize the spatial dependency. By solving this equation, it is possible to obtain the desired elevation values that satisfy the given condition.

From there, it follows that each corresponding elevation value of the pixel (i, j) will be adjusted by a value given by:

$$du_{ij}^{sd} = v_{ij}^{expected} - v_{ij} \quad (3),$$

In equation (3), du_{ij}^{sd} represents the adjusted elevation value for the pixel (i,j) by the principle of spatial dependency maximization. It is calculated by taking the expected elevation value, $v_{ij}^{expected}$, and subtracting the original elevation value, v_{ij}. This adjustment helps to refine and improve the elevation values of the sub-pixels in the downscaled DEM.

The adjustment process will be iterated repeatedly until the variogram values reach a minimum at every pixel (i,j). This result corresponds to the scenario where the elevation values of all sub-pixels in the DEM will be equal to the average of the elevation values of surrounding sub-pixels.

It can be observed that if only the principle of maximizing spatial dependency, as described above, is applied to the DEM, the elevation values of the sub-pixels in the final DEM will be equal. Therefore, another function is needed, called the elevation constraint. The principle of this constraint is that the average elevation of the sub-pixels within the range of an original pixel in the original DEM should be equal to the elevation value of that pixel in the original DEM.

Thus, the elevation constraint function will have the following value:

$$du_{ij}^{ep} = Elevation_{x,y} - \frac{\sum_{(x-1)f}^{xf} \sum_{(y-1)f}^{yf} v_{pq}}{f \times f} \quad (4),$$

In equation (4), du_{ij}^{ep} represents the adjustment value based on the elevation constraint for the sub-pixel (i,j). It is calculated by subtracting the average of the elevation values of all sub-pixels within the footprint of the original pixel (x,y) in the original image from the elevation value of that pixel in the original DEM. This adjustment helps to ensure that the final accuracy enhanced DEM satisfies the elevation constraint, maintaining consistency with the original DEM in terms of average elevation values in each original pixel. With $Elevation_{x,y}$ representing the elevation of the pixel (x,y) in the original DEM that contains the pixel (i,j), and (p,q) representing the sub-pixels within the coverage area of the pixel (x,y), the adjustment value for the elevation of each sub-pixel in the enhanced high-resolution DEM after each iteration will be given by:

$$du_{ij} = du_{ij}^{sd} + du_{ij}^{ep} \quad (5)$$

With g being the activation function in neural network

models, and in this model using a linear activation function, the elevation values of the image points (sub-pixel) after each iteration *t* will be equal to

$$v_{ij}^{t} = g\left(v_{ij}^{t-1}\right) = au_{ij} + b \quad (6).$$

In equation (6), v_{ij}^{t} represents the elevation value of the pixel (*i,j*) at iteration *t*. It is calculated by applying the activation function g to the elevation value at a previous iteration v_{ij}^{t-1}, which results in a linear transformation represented by the coefficients *a* and *b*.

The HNN is a type of recurrent network that runs through multiple iterations until it reaches the desired target value. In the proposed HNN model by (Minh & Huong, 2013), the expected target is determined by:

$$E = \sum_i \sum_j \left(du_{ij}^{sd} + du_{ij}^{ep}\right) = min \quad (7),$$

where *E* is the energy function. The energy function represents the summation of the goal function and constraint values. When energy function value *E* is minimized, the neural network stops iterating, and the elevation value at the point of network convergence is taken as the final elevation value for the sub-pixels in the high-resolution DEM.

2.2 HNN downscaling DEM with additional point data

The new HNN model proposed for incorporating supplementary elevation data is developed upon the previously mentioned HNN DEM downscaling model. In this model, a pixel in the original DEM was also divided into *f*×*f* sub-pixels. The principle of this new HNN model is presented in Fig 2.

Let's consider a supplementary elevation point located at sub-pixel position (*k*,*l*), with an elevation value of $Elev_{Supplementary}$, while the corresponding elevation value in the original DEM is $Elev_{Original}$. At each sub-pixel position that contains a supplementary elevation point, the adjustment value for elevation can be determined as:

$$\Delta Elev^{Expected} = Elev_{Supplementary} - Elev_{Original} \quad (8).$$

For the remaining sub-pixels in the downscaled DEM, the adjustment values for elevation from the supplementary data are determined using a similar principle as described in Equation (4), where the adjustment values for neighboring sub-pixels are expected to be similar. Therefore, the adjustment value for elevation at sub-pixel (*i*, *j*) is determined as:

$$\Delta Elev_{ij}^{Expected} = \frac{\sum_1^{N(h)} \Delta Elev_{ij+h}}{N(h)} \quad (9).$$

where $\Delta Elev_{ij}^{Expected}$ represents the adjustment value for elevation determined from a group of supplementary elevation points. Here, *h* denotes the distance between sub-pixel (*i*, *j*) and its neighboring sub-pixels. In this model, *h* = 1 indicates that the considering only the sub-pixels that are adjacent to sub-pixel (i,j). $\Delta Elev_{ij+h}$ represents the adjustment value for elevation of the neighboring pixels, and *N*(*h*) is the number of sub-pixel pairs. In the case of considering only the sub-pixels

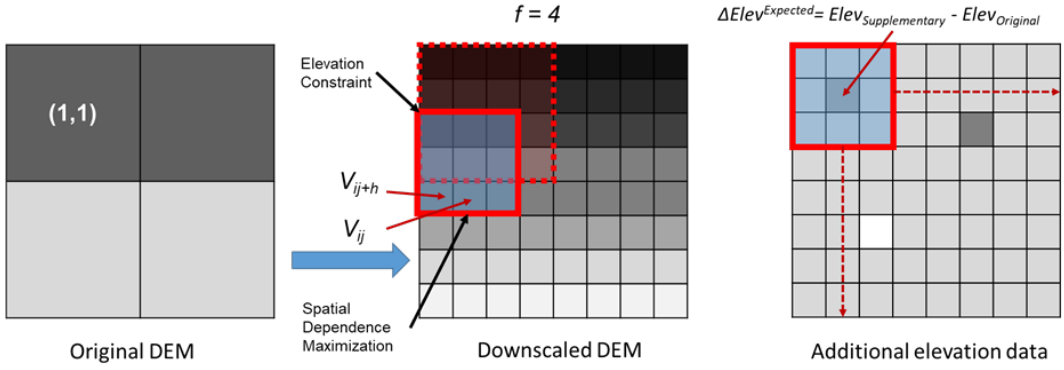

Fig. 2 New model of downscaling using Hopfield Neural Network with additional elevation data.

in direct contact with sub-pixel (*i*,*j*), the maximum number of sub-pixel pairs is 8. Please note that the adjustment presented in Equation 9 is not used for the sub-pixels containing the supplementary elevation points.

The value of the elevation adjustment from the additional elevation points at each iteration *t* for each pixel is given by:

$$du_{ij}^{\Delta Elev} = \Delta Elev_{ij}^{Expected} - \Delta Elev_{ij}^{t} \quad (10),$$

where $du_{ij}^{\Delta Elev}$ is the calculated adjustment value from the additional control points, and $\Delta Elev_{ij}^{t}$ is the elevation adjustment value for each sub-pixel at the t^{th} iteration.

Due to the presence of the elevation adjustment function from the additional control points, the constraint function also needs to be adjusted. It is assumed that all sub-pixels within the range of a pixel (*x*,*y*) belonging to the original elevation model are adjusted by a value of $\Delta Elev_{pq}^{t}$ Therefore, the height value of pixel (*x*,*y*) will be adjusted by:

$$\Delta Elev_{x,y} = \frac{\sum_{(x-1)f}^{xf}\sum_{(y-1)f}^{yf}\Delta Elev_{pq}^{t}}{f \times f} \quad (11),$$

where *f* is zooming factor. The value of the elevation constraint will be determined by:

$$du_{ij}^{ep} = Elevation_{x,y} - \frac{\sum_{(x-1)f}^{xf}\sum_{(y-1)f}^{yf} v_{pq}}{f \times f} + \frac{\sum_{(x-1)f}^{xf}\sum_{(y-1)f}^{yf}\Delta Elev_{pq}^{t}}{f \times f} \quad (12)$$

Thus, the total height adjustment value from Equation (7) will be determined by:

$$du_{ij} = du_{ij}^{sd} + du_{ij}^{ep} + du_{ij}^{\Delta H} \quad (13).$$

The energy function *E* of the HNN is adjusted and used as a condition to complete the iteration process as follows:

$$E = \sum_i \sum_j \left(du_{ij}^{sd} + du_{ij}^{ep} + du_{ij}^{\Delta Elev} \right) = min \quad (14).$$

3. Data

To evaluate the proposed algorithm for DEM downscaling, a DEM model for a small area in Cao Bang Province was used for testing. The data was downloaded from the website of the US Geological Survey (https://earthexplorer.usgs.gov/) for the Cao Bang Province area, consisting of two pieces of elevation data in GeoTIFF format with the filenames n22_e105_1arc_v3 and n22_e106_1arc_v3. The location and coverage of these elevation models are presented in Fig. 3. The data is georeferenced with EPSG:32648 - WGS 84/UTM zone 48N coordinate system and the elevation is based on the global geoid model EGM96. The data was established in 2011 with a spatial resolution of 30 meters.

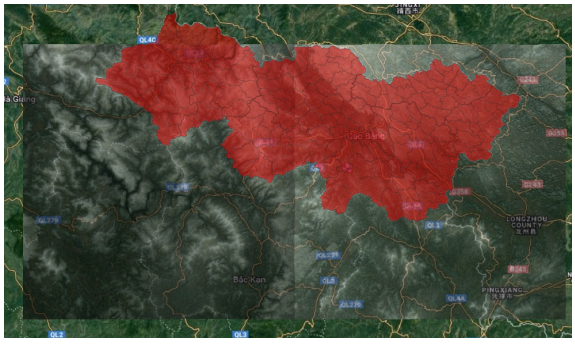

Fig. 3 STRM data of Cao Bang Province

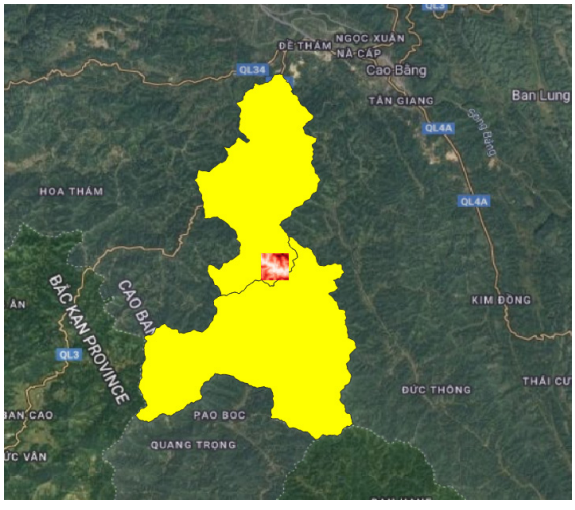

Fig. 4 Location of the DEM used for evaluation of the newly proposed algorithm between Bach Dang commune, Hoa An district and Minh Khai commune, Thach An district, Cao Bang Province.

The accuracy of the elevation data has been evaluated in various relatively different areas within a range of ±6 meters

to ±9 meters (Chen *et al.*, 2020; Mukul *et al.*, 2017). For mountainous areas similar to Cao Bang, it is possible to estimate that the RMSE (Root Mean Square Error) of DEM is approximately ±9 meters. The elevation data from the global geoid model is adjusted to the elevation system of Vietnam based on the geoid benchmark at Hon Dau tidal station, Hai Phong, using the height difference values determined by (Hoa, 2017), where the global model elevation values are adjusted by the height difference D0 = 0.890 meters. The supplementary elevation points data is derived from the 1:10,000 topographic base data established in 2012 through photogrammetric surveying with a contour elevation interval of 5 meters, and the RMSE is determined according to the regulations specified in Circular 12/2020/TT-BTNMT (2020), which is one-third of the contour elevation interval (increased by 1.5 times under special difficult conditions). The accuracy of the elevation points corresponds to a RMSE of ±2.5 meters.

4. Experiment

The proposed algorithm was tested on a pierce of DEM data in an area of 1650 m × 1344 m (Fig. 4) with its center located at coordinates 106.71580E, 22.553640N (according to the EPSG:32648 - WGS 84 / UTM zone 48N coordinate system). The location of the testing DEM is located in Bach Dang Commune, Hoa An District and Minh Khai Commune, Thach An District in Cao Bang Province.

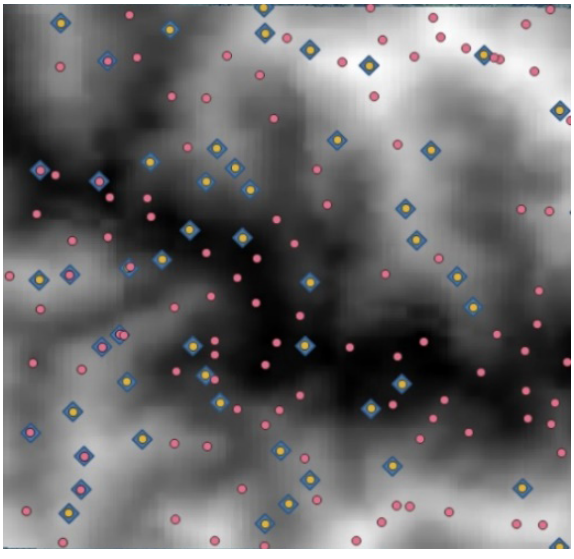

Fig. 5 Supplementary elevation data: Additional elevation points for DEM improvement, Elevation points for accuracy evaluation

The supplementary elevation points in the experimental area were extracted from the 1:10000 scale geospatial information dataset. The elevation points were divided into two groups: a group of 130 points used to enhance the accuracy of the elevation model, and a group of 64 points used to evaluate the algorithm's accuracy. The distribution of these point groups is shown in Fig. 5.

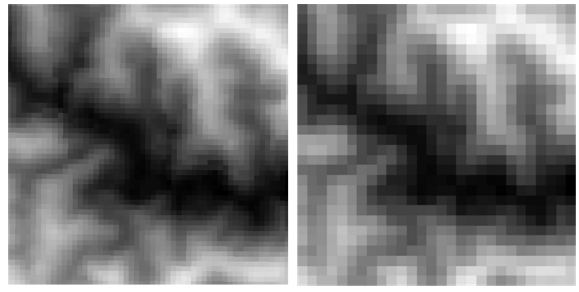

(a) (b)

Fig. 6 DEM datasets used as input for HNN downscaling models: (a) SRTM 30 m resolution data, (b) Downgraded 60 m resolution DEM

To evaluate the algorithm, DEMs at different resolutions were used as input for the HNN model to enhance the resolution with 130 supplementary elevation points. An original SRTM 30 m elevation model data DEM (presented in Fig. 6(a)) was used as input for the HNN model to generate 7.5 m DEM (zoom factor $f = 4$). The results of the downscaling using the new HNN model are presented in Fig. *7*(b). Additionally, the elevation model data was also downscaled using the conventional HNN model, (without the inclusion of additional elevation points), bilinear and bi-cubic resampling for evaluation purposes, and the results are shown in Figs. *7*(c), (d) and (e), respectively

The original STRM DEM was also downgraded to 60 m resolution using average method and this DEM was used as input for the new HNN downscaling to produce the DEMs at resolutions of 30 m, 20 m, 15 m, 12 m and 10 m, corresponding to the zoom factors of 2, 3, 4, 5 and 6, respectively. These

would help to evaluate the effect of zoom factors of the newly proposed HNN downscaling using supplementary elevation data. The input DEM datasets are presented in Fig. 6(b) and the resulted downscaled DEMs of both HNN downscaling and proposed HNN downscaling with supplementary data are presented in the Figs. 8(a), 8 (b) for DEMs at 30 m resolution, Fig. 8(c) and Fig. 8(d) for DEM at 20 m resolution, Figs. 9(a), 9(b) for DEM at 15 m resolution, Figs. 9(c), 9(d) for DEM at 12 m resolution, and Figs. 9(e) , 9(f) for DEM at 10 m resolution.

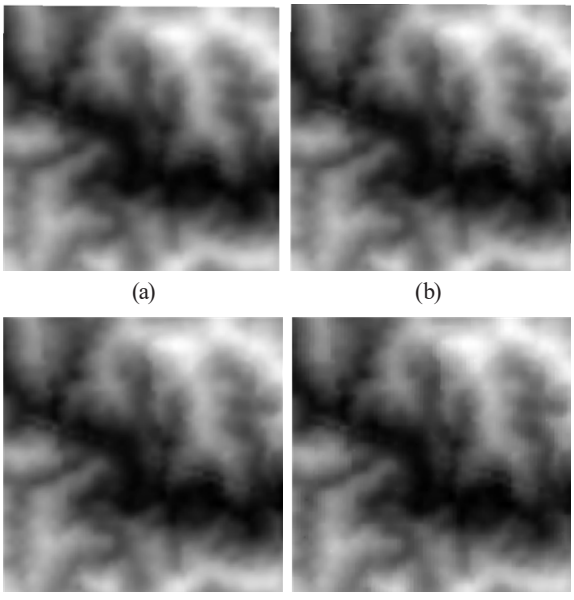

(a) (b) (c) (d)

Fig. 7 Results of resampling and downscaling of 30 m SRTM DEM with zoom factor of 4 to 7.5 m resolution: (a) result of bilinear method; (b) result of bi-cubic method; (c) results of HNN; (d) results of new HNN with supplementary elevation data.

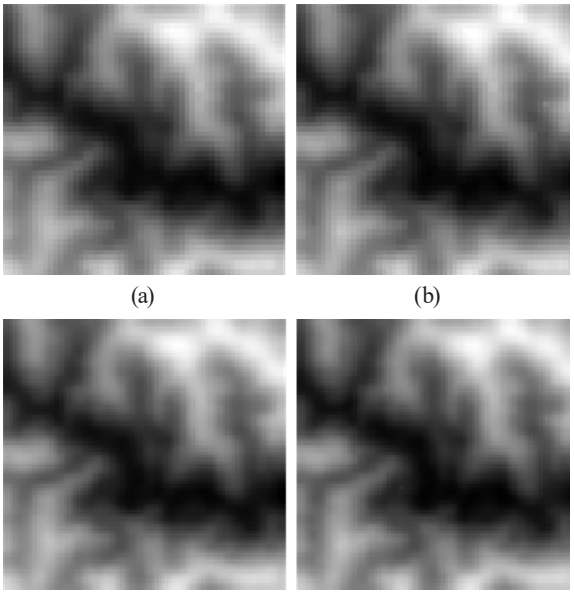

(a) (b) (c) (d)

Fig. 8 Results of downscaling of 60 m degraded SRTM DEM with zoom factor of 2 to 30 m resolution and factor of 3 to 20 m resolution: (a) 30 m HNN downscaled DEM; (b) 30 m new HNN downscaled DEM (c) 20 m HNN downscaled DEM; (d) 20 m new HNN downscaled DEM.

5. Results and discussion

To evaluate the results of the algorithm that improves the accuracy of the elevation model using the HNN with additional elevation points, a dataset of 64 points was used, and the performance of the algorithms was assessed using parameters including RMSE and Mean Absolute Error (MAE). The evaluation results are presented in Table 1. In this dataset, the elevations of the test points are compared with the elevations obtained from the SRTM 30 m DEM, the 7.5 m resolution DEM generated by conventional resampling methods such as bilinear and bi-cubic, the Hopfield neural network without additional elevation points, and the 7.5 m resolution elevation model generated by the Hopfield neural network with additional elevation points. The purpose of this is to assess the newly proposed HNN downscaling algorithm by comparing it′s accuracy statistics to those of the conventional resampling and downscaling algorithms.

The results in Table 1 show that when comparing the maximum and minimum error values, the use of additional elevation data has corrected the larger errors. The absolute values of both the smallest and largest errors have decreased for the elevation model produced by the HNN with the use of additional elevation points. Comparing the results in terms of RMSE and MAE indicates a significant improvement in accuracy when incorporating additional elevation points

into the HNN model compared to the resampling by bilinear and bi-cubic, and HNN downscaling without additional points cases. The RMSE has decreased from ±9.197 m, ±9.122 m, ±9.595 m and ±9.234 m for the original DEM, the elevation model generated by the HNN downscaling, bilinear and bi-cubic resampling, respectively, to ±6.490 when supplementary elevation data was incorporated in the model. Thus, using the supplementary elevation data will help the accuracy of the DEM increased by nearly 30% compared to the original model and 29% compared to the DEM generated by the HNN DEM downscaling without additional elevation points.

Table 1. Accuracy assessment for HNN downscaling and HNN downscaling using supplementary elevation points for SRTM DEM at 30 m.

Dataset	Resolution (m)	Errors			
		Min (m)	Max (m)	RMSE (m)	MAE (m)
SRTM 30 m	30.0	-28.5	18.6	±9.197	7.431
DEM 7.5 m resampled using bilinear	7.5	-28.5	19.2	±9.595	7.830
DEM 7.5 m resampled using bi-cubic	7.5	-28.5	19.2	±9.234	7.447
DEM 7.5 m downscaled using HNN	7.5	-28.231	19.294	±9.122	7.319
DEM 7.5 m downscaled using HNN with supplementary elevation data	7.5	-15.371	13.987	±6.490	5.140

Similarly, comparing the MAE (Mean Absolute Error) values of the DEMs also demonstrates a significant reduction in the MAE for the 7.5 m resolution DEM generated by the HNN with additional elevation points compared to the original 30 m resolution DEM (SRTM 30 m), the HNN downscaling without using supplementary data, bilinear and bi-cubic resampling approaches. The values of MAE reduced from 7.830 m, 7.447 m, and 7.319 m for the DEM produced by bilinear, bi-cubic and HNN downscaling, respectively, to 5.140 m for the DEM produced by HNN downscaling with supplementary data.

Although the DEM by the conventional resampling and HNN downscaling achieved an improvement in accuracy when compared to the original SRTM elevation model, the MAE only decreased by 0.12 m for this DEM. However, when using additional elevation points, the MAE decreased by 2.2 m from 7.319 m for the elevation model generated by the HNN without additional elevation points to 5.140 m, thanks to the incorporation of additional elevation points.

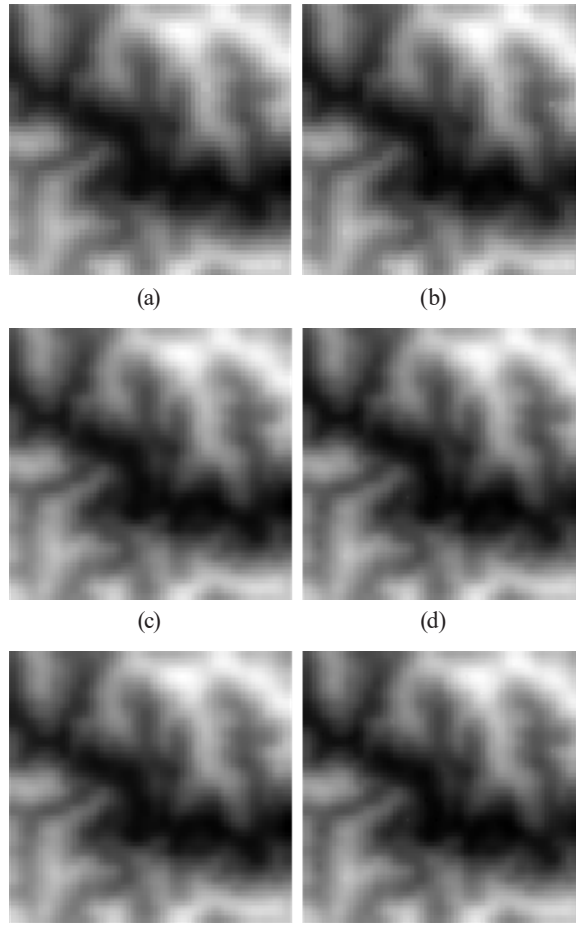

Fig. 9 Results of downscaling of 60 m degraded SRTM with zoom factor of 4, 5, 6: (a) 15 m HNN downscaled DEM; (b) 15 m new HNN; (c) 12 m HNN downscaled DEM; (d) 12 m new HNN downscaled DEM; (e) 10 m HNN downscaled DEM; (d) 10 m new HNN downscaled DEM.

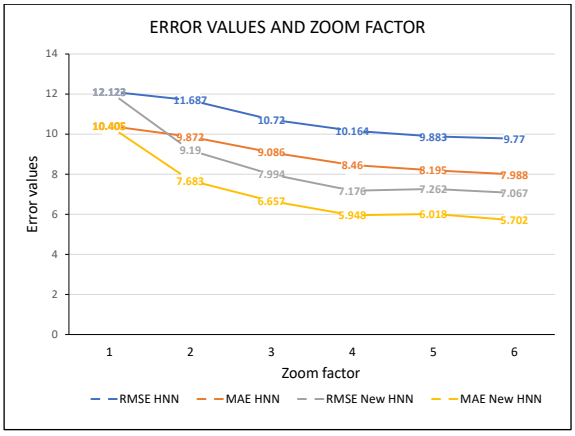

Fig. 10 Changes of error values versus zoom factor

To investigate the effects of zoom factor to the newly proposed algorithm, the downscalings of DEM using HNN and HNN with additional point data were implemented using zoom factors ranging from 2 to 6. Resulting downscaled DEMs are presented in Figs. 8 and 9. The evaluation of this DEMs is based on basic statistics such as RMSE and MAE with a set 64 validation elevation points (Fig.5) and presented in Table 2. Additionally, Fig. 10 illustrate the variation in accuracy as a function of the zoom factor. These variations show a correlation between zoom factor and the accuracy of the downscaled DEMs. As the zoom factor increases, the accuracy of both HNN downscaling and HNN downscaling using supplementary elevation data is increased. The RMSE of HNN downscaled DEM reduced from ±12.123 m of original 60 m DEM to ±11.687 m, ±10.720 m, ±10.164 m, ±9.883 m and ±9.770 m for DEMs with zoom factor of 2, 3, 4, 5 and 6, respectively. Similarly, when incorporating supplementary elevation data to the HNN, the RMSE of the DEM decreased to ±9.190 m, ±7.994 m, ±7.176 m, ±7.262 m, and ±7.067 m. Upon inspection, it is evident that the incorporation of supplementary elevation data significantly enhances the accuracy of the DEM compared to using HNN downscaling alone, without supplementary elevation data. The most accurate DEM achieved through HNN downscaling showed an improvement of approximately 20% compared to the original low-resolution DEM. However, with the newly proposed HNN algorithm, the accuracy of the most accurate DEM improved by approximately 41.5% in comparison to the original DEM.

Although the accuracy of the DEM improves as the zoom factor increases, there appears to be a limitation in the extent of accuracy improvement for two HNN-based downscaling

Table 2. Accuracy assessment for HNN downscaling and HNN downscaling using supplementary elevation points for downgraded DEM at 60 m

Dataset	Resolution (m)	Errors			
		Min (m)	Max (m)	RMSE (m)	MAE (m)
Downgraded SRTM 60 m	60.0	-30.5	22.6	±12.123	10.405
DEM 30 m downscaled with HNN	30.0	-30.12	22.0	±11.687	9.872
DEM 30 m downscaled using HNN with supplementary elevation data	30.0	-16.867	18.366	±9.190	7.683
DEM 20 m downscaled with HNN	20.0	-27.967	20.864	±10.720	9.086
DEM 20 m downscaled using HNN with supplementary elevation data	20.0	-17.407	17.384	±7.994	6.657
DEM 15 m downscaled with HNN	15.0	-27.403	21.41	±10.164	8.460
DEM 15 m downscaled using HNN with supplementary elevation data	15.0	-12.787	15.918	±7.176	5.948
DEM 12 m downscaled with HNN	12.0	-26.521	19.827	±9.883	8.195
DEM 12 m downscaled using HNN with supplementary elevation data	12.0	-13.6	16.279	±7.262	6.018
DEM 10 m downscaled using HNN	10.0	-26.0	19.9	±9.770	7.988
DEM 10 m downscaled using HNN with supplementary elevation data	10.0	-13.415	17.618	±7.067	5.702

methods. Specifically, when the zoom factor is increased to 4, the HNN downscaling method results in an RMSE and MAE reduction of approximately 1.96 m and 1.945 m, respectively. However, when the zoom factor is further increased from 4 to 6, the reduction in RMSE and MAE is only around 0.4 m and 0.5 m, respectively. Similarly, for the HNN downscaling method using supplementary data, a reduction of approximately 4.95 m in RMSE and 4.46 m in MAE is observed when the zoom factor is increased to 4. In contrast, when the zoom factor is increased from 4 to 6, the reduction in RMSE and MAE is merely 0.11 m and 0.25 m, respectively. These findings suggest that a zoom factor of 4 appears to be the most optimized value for the model, as it achieves a balance between accuracy improvement and the diminishing returns observed at higher zoom factors.

6. Conclusions

Although the HNN has demonstrated the ability to improve the accuracy of elevation models when used to enhance the resolution of grid-based DEMs, it is necessary to further enhance the HNN model by integrating additional elevation data when available. The results of the study have shown that the proposed HNN DEM downscaling model, designed to incorporate supplementary elevation data, has significantly improved the accuracy of the DEM. Both the Root Mean Square Error and Mean Absolute Error values have decreased significantly, and the accuracy of the DEM has increased by from 30% to 40% compared to the original models.

Additionally, the findings indicate that a zoom factor of 4 appears to be the optimal choice for the newly proposed models. This zoom factor strikes the best balance between accuracy and computing cost as the zoom factor increases.

Although the proposed model has only been tested on a relatively small dataset, the promising results of using the HNN model to integrate available elevation data for improving the accuracy of elevation models, especially for global elevation datasets like SRTM 30 m data, indicate that the proposed method can be applied in practical settings with comprehensive evaluations under various terrain conditions.

Acknowledgement

The content of this scientific paper presents the research findings of the project with the code B2021-MDA-04, funded by the Ministry of Education and Training. The authors would like to express their sincere gratitude to the Ministry of Education and Training and the Hanoi University of Mining and Geology for providing the necessary resources and support to successfully complete this research.

References

Bhuyian, M., J., Kalyanapu, A., & Fernando, N. (2015), Approach to Digital Elevation Model Correction by Improving Channel Conveyance. *Journal of Hydrologic Engineering*, Vol 20, No. 5, 4014062. https://doi.org/10.1061/(ASCE)HE.1943-5584.0001020

Chen, C., Yang, S., & Li, Y. (2020), Accuracy Assessment and Correction of SRTM DEM Using ICESat/GLAS Data under Data Coregistration, In *Remote Sensing* (Vol. 12, No. 20). https://doi.org/10.3390/rs12203435

Courty, L. G., Soriano-Monzalvo, J. C., & Pedrozo-Acuña, A. (2019), Evaluation of open-access global digital elevation models (AW3D30, SRTM, and ASTER) for flood modelling purposes, *Journal of Flood Risk Management*, Vol. 12, No S1, pp. 1–14. https://doi.org/10.1111/jfr3.12550

Grohmann, C. H., & Steiner, S. S. (2008), SRTM resample with short distance-low nugget kriging, *International Journal of Geographical Information Science*, Vol. 22, No. 8, pp. 895–906. https://doi.org/10.1080/13658810701730152

Hoa, H. M. (2017), Construction of initial national quasi-geoid model VIGAC2017, first step to national spatial reference system in Vietnam, *Vietnam Journal of Earth Sciences. 2017a*, Vol. 39, No. 2, pp. 155–166.

Jana, R., Reshmidevi, T. V, Arun, P. S., & Eldho, T. I. (2007), An enhanced technique in construction of the discrete drainage network from low-resolution spatial database, *Computers & Geosciences*, Vol 33, No. 6, pp. 717–727.

https://doi.org/10.1016/j.cageo.2006.06.002

Minh, N. Q., & Huong, N. T. T. (2013), Increasing spatial resolution of remotely sensed image using HNN Super-resolution mapping combined with a forward model, *Journal of the Korean Society of Surveying Geodesy Photogrammetry and Cartography*, Vol. 31, No. 6 PART 2. https://doi.org/10.7848/ksgpc.2013.31.6-2.559

Circular 12/2020/TT-BTNMT on national topographic maps of 1:10000 and 1:25000.

Mukul, M., Srivastava, V., Jade, S., & Mukul, M. (2017), Uncertainties in the Shuttle Radar Topography Mission (SRTM) Heights: Insights from the Indian Himalaya and Peninsula, *Scientific Reports*, Vol. 7, No. 1, 41672. https://doi.org/10.1038/srep41672

Nguyen, M. Q., Atkinson, P. M., & Lewis, H. G. (2006), Superresolution mapping using a hopfield neural network with fused images, *IEEE Transactions on Geoscience and Remote Sensing*, Vol 44, No. 3, 736–749. https://doi.org/10.1109/TGRS.2005.861752

Nguyen, Q. M., Nguyen, T. T. H., La, P. H., Lewis, H. G., & Atkinson, P. M. (2019), Downscaling Gridded DEMs Using the Hopfield Neural Network, *IEEE Journal of Selected Topics in Applied Earth Observations and Remote Sensing*, Vol 12, No. 11, pp. 4426–4437. https://doi.org/10.1109/JSTARS.2019.2953515

Paredes-Hernández, C. U., Tate, N. J., Tansey, K. J., Fisher, P. F., & Salinas-Castillo, W. E. (2010), Increasing the Accuracy of Low Spatial Resolution Digital Elevation Models using Geostatistical Conflation, *Ninth International Symposium on Spatial Accuracy Assessment in Natural Resources and Environmental Sciences*, pp. 413–416.

Pham, H. T., Marshalla, L., Johnsona, F., & Sharmaa, A. (2018), A method for combining SRTM DEM and ASTER GDEM2 to improve topography estimation in regions without reference data, *Remote Sensing of Environment, 210*, 229–241. https://doi.org/10.1016/J.RSE.2018.03.026

Tang, Y., Zhang, J., Li, H., Ding, H., Liu, J., & Jing, L. (2014), A multiple-point geostatistical method for digital elevation models conflation. *International Geoscience and Remote Sensing Symposium (IGARSS)*, pp. 4299–4302. https://doi.org/10.1109/IGARSS.2014.6947440

Uuemaa, E., Ahi, S., Montibeller, B., Muru, M., & Kmoch, A. (2020), Vertical Accuracy of Freely Available Global Digital Elevation Models (ASTER, AW3D30, MERIT, TanDEM-X, SRTM, and NASADEM), In *Remote Sensing* Vol. 12, No. 21. https://doi.org/10.3390/rs12213482

Wu, S., Li, J., & Huang, G. H. (2008), A study on DEM-derived primary topographic attributes for hydrologic applications: Sensitivity to elevation data resolution, *Applied Geography*, Vol 28, No 3, pp. 210–223. https://doi.org/10.1016/j.apgeog.2008.02.006

Yamazaki, D., Ikeshima, D., Tawatari, R., Yamaguchi, T., O'Loughlin, F., Neal, J. C., Sampson, C. C., Kanae, S., & Bates, P. D. (2017), A high-accuracy map of global terrain elevations. *Geophysical Research Letters*, Vol. 44, No. 11, pp. 5844–5853. https://doi.org/https://doi.org/10.1002/2017GL072874